Article

Pneumocytes Assemble Lung Surfactant as Highly Packed/Dehydrated States with Optimal Surface Activity

Alejandro Cerrada,[1] Thomas Haller,[2] Antonio Cruz,[1] and Jesús Pérez-Gil[1,*]
[1]Department of Biochemistry, Faculty of Biology, and Hospital 12 Octubre Research Institute, Universidad Complutense, Madrid, Spain; and
[2]Department of Physiology and Medical Physics, Medical University of Innsbruck, Innsbruck, Austria

ABSTRACT Pulmonary surfactant (PS) is an essential complex of lipids and specific proteins synthesized in alveolar type II pneumocytes, where it is assembled and stored intracellularly as multilayered organelles known as lamellar bodies (LBs). Once secreted upon physiological stimulation, LBs maintain a densely packed structure in the form of lamellar body-like particles (LBPs), which are efficiently transferred into the alveolar air-water interface, lowering surface tension to avoid lung collapse at end-expiration. In this work, the structural organization of membranes in LBs and LBPs freshly secreted by primary cultures of rat ATII cells has been compared with that of native lung surfactant membranes isolated from porcine bronchoalveolar lavage. PS assembles in LBs as crystalline-like highly ordered structures, with a highly packed and dehydrated state, which is maintained at supraphysiological temperatures. This relatively ordered/packed state is retained in secreted LBPs. The micro- and nanostructural examination of LBPs suggests the existence of high levels of structural complexity in comparison with the material purified from lavages, which may contain partially inactivated or spent structures. Additionally, freshly secreted surfactant LBPs exhibit superior activity when generating interfacial films and a higher intrinsic resistance to inactivating agents, such as serum proteins or meconium. We propose that LBs are assembled as an energy-activated structure competent to form very efficient interfacial films, and that the organization of lipids and proteins and the properties displayed by the films formed by LBPs are likely similar to those established at the alveolar interface and represent the actual functional structure of surfactant as it sustains respiration.

INTRODUCTION

The alveolar spaces of mammalian lungs are lined by a thin layer of water coated with a macromolecular lipid-protein complex, the pulmonary surfactant (PS) (1). PS is essential for breathing as it reduces the surface tension at the lung's air-liquid interface, thus preventing atelectasis (alveolar collapse), particularly at the end of expiration (2–4). Additionally, PS is also an important component of the innate immune defense system in the lung (5–7) and it has been described to facilitate oxygen diffusion through the thin water layer covering the respiratory surface (8). It is composed of phospholipids (80%), neutral lipids (mainly cholesterol, 8–10%), and surfactant-associated proteins (10%) (1,9,10).

Surfactant components are produced in specialized cells of the alveolar epithelium, the alveolar type II cells. The protein components are synthesized in the endoplasmic reticulum, processed in the Golgi apparatus and late endosomes/multivesicular bodies and partly assembled in the intracellular storage organelles known as lamellar bodies (LBs), whereas surfactant lipids may traffic directly from the endoplasmic reticulum into LBs (1,11,12). LBs are lysosome-related vesicles with an acidic interior pH of ~6 (13). Proteomic profiling of LBs reveals a highly dynamic organelle containing proteins corresponding to different functional categories, mainly with lipid-related functions and involved in the biosynthetic, secretory, and endocytic pathways of PS (14,15). Interestingly, the lipid importer ABCA3 has been proposed to play a key role in surfactant biogenesis incorporating phosphatidylcholine (PC) and phosphatidylglycerol (PG) through the limiting membrane of LBs into their lumen (14,16). Deficiencies in this transporter are associated with some respiratory syndromes of variable severity (17). By transmission electron microscopy, LBs appear as osmiophilic vesicles containing tightly packed, relatively periodically arranged lamellae, surrounded by an outer limiting membrane (11).

Exocytosis of LBs is a constitutive and regulated process, which can be stimulated by certain chemical or physical factors (18–21). Upon secretion, LBs are released as dense particulate entities (lamellar body-like particles, LBPs), which remain in a compact state until reaching the alveolar air-liquid interface (22). Once LBPs contact the interface, they disintegrate leading to an instantaneous spreading of material and the formation of a surface-active film (26). It has been recently reported how the adsorptive capacity of LBPs into an air-liquid interface is affected by some physicochemical parameters, such as pH and temperature (23). A particularly dramatic impact on interfacial adsorption was seen by the proteolytic treatment of LBPs, suggesting the importance of surfactant proteins. We have previously described that the films formed by adsorbed LBPs exhibit a lateral structural heterogeneity manifested by a lipid phase coexistence with segregated ordered and disordered regions (24). In addition,

Submitted April 15, 2015, and accepted for publication October 13, 2015.
*Correspondence: jperezgil@bio.ucm.es
Editor: Arne Gericke.

0006-3495/15/12/2295/12
http://dx.doi.org/10.1016/j.bpj.2015.10.022

progressive adsorption of LBPs leads to the appearance of large protruded three-dimensional (3D) complex structures as well as a stiffening and solidification of the ensuing surface films. Interestingly, the solid-like character and the 3D structures associated with the film are not observed upon adsorption of surfactant purified from bronchoalveolar lavage (BAL) (24). These findings suggested that surfactant derived from animal BAL, which is typically used as a standard material and a reference for optimal surfactant function, could only partially represent the properties of the film existing in the alveolar spaces, preventing a proper interpretation of the structure and behavior of surfactant in the native situation. In fact, material from lavage likely contains partially inactivated complexes (already spent, or oxidized), and possibly structures from locations in the airways different than alveolar spaces and/or related with other functions.

In this work and to further investigate the genuine structural organization of LBPs, we have assessed packing and hydration properties of surfactant stored in intracellular LBs as well as in LBPs secreted by primary cultures of rat ATII cells in comparison with that of native lung surfactant membranes isolated from porcine BAL. We propose that the structures and activities exhibited by material assembled and freshly secreted by primary cells is more likely to represent the real situation at the alveolar spaces. We have also analyzed the nanostructural features of adsorbed LBPs as well as their response to inhibitory agents in terms of surface activity and stability. Our findings corroborate the existence of significant structural differences between both types of surfactant organizations and their correlation with functional efficiency at the air-liquid interface.

MATERIALS AND METHODS

Reagents

ATP, phorbol 12-myristate 13-acetate, Brilliant Black (BB), salts, and chemicals were purchased from Sigma (Sigma-Aldrich Química, Madrid, Spain). 1,1-Dioctadecyl-3,3,3,3-tetramethylindocarbocyanine perchlorate (DiIC 18) and 2-(4,4-difluoro-5,7dimethyl-4-bora-3a,4a-diaza-sindacene-3pentanoyl)-1-hexadecanoyl-sn-glycero-3phosphocholine (Bodipy-PC) were from Molecular Probes (Eugene, OR). The phospholipid quantitation kit was purchased from Spinreact (Girona, Spain).

Cell preparation

Alveolar type II (ATII) cells were isolated from the lungs of anesthetized male Sprague-Dawley rats as introduced by Dobbs et al (25) with minor modifications as described elsewhere (26). Upon isolation and purification, cells were seeded in petri dishes and maintained for 3 days in Dulbecco's modified Eagle's medium culture supplemented with fetal calf serum and antibiotics.

Surfactant preparations

This work establishes a systematic comparison of the behavior of surfactant freshly secreted by primary cultures of rat type II cells and surfactant complexes purified from porcine BAL. In our extensive experience, surfactant material from different mammal species such as rats, mice, or pigs has a similar compositional framework and a very consistent behavior. We therefore assume that the comparison between the materials studied here may reveal relevant features of different surfactant stages, on top of more negligible interspecific differences. Exocytosis and release of LBPs was stimulated by incubation of adherent ATII cells with ATP (100 μM) and phorbol 12-myristate 13-acetate (500 nM) in buffered solution (containing, in mM: NaCl 140, KCl 5, $MgCl_2$ 1, $CaCl_2$ 2, HEPES 10, pH 7.4 supplemented with 0.1 mg/ml streptomycin and 100 units/ml penicillin) as previously described (25). After 6 h of stimulation at 37°C, supernatants containing released LBPs were harvested, aliquoted, and stored at −20°C until use. Electron microscopy examination revealed that this material is rich in densely packed multilamellar structures (the LBP particles) but contain no tubular myelin figure (24). Native surfactant from BALs of slaughtered porcine adult fresh lungs was purified and separated from blood components by NaBr density-gradient centrifugation as described (27). It contains all the components assembled and secreted into the lipid-protein complexes synthetized by the pneumocytes, including the lipids and the hydrophilic (SP-A) and hydrophobic proteins. The organic extract (OE) from porcine native surfactant purified from lavage (containing all the surfactant lipids plus the hydrophobic proteins SP-B and SP-C; composition characterized in detail elsewhere (28)) was obtained by chloroform/methanol (2:1 v/v) extraction (29). To obtain an aqueous suspensions of OE, the required volume of the extract was first dried under nitrogen and then under vacuum using the equipment from UNIVAP for 2 h to remove traces of solvent, and then hydrated in buffer 5 mM Tris pH 7, 150 mM NaCl for 1 h at 45°C. Phospholipid content was measured by phosphorous quantitation (30) or by enzymatic detection (31). Cholesterol in NS and OE samples has been calculated to be around 8% by mass with respect to phospholipids, as determined by a cholesterol oxidase enzymatic assay (28). The proportion of cholesterol in LBPs is closer to 5%.

Laurdan fluorescence

NS, OE, and suspensions of secreted LBPs were stained with the fluorescent probe Laurdan (6-lauroyl, 1-2-dimethylamino naphthalene) for 1 h at 37°C in a proportion of 1% (mol/mol) with respect to phospholipids as previously described (28,32). Typically, the fluorescent probe is added as a small aliquot (0.5 μL) of a dimethylsulphoxide (DMSO) concentrated solution into a much larger solution ($\geq$0.5 mL) of buffer or culture medium. No apparent effects were detected upon the addition of an equivalent aliquot of pure DMSO (i.e., in the infrared (IR) spectra). For the staining of intracellular LBs, ATII cells grown on glass coverslips were incubated with 100 μM Laurdan in Dulbecco's modified Eagle's medium for 1 h at 37°C. In the case of the suspensions, the fluorescence spectra of all samples were recorded in a temperature-controlled AmincoBowman Series 2 luminescence spectrometer, using an excitation wavelength of 370 nm and recording the emission spectrum between 400 and 550 nm, within a temperature range of 10–60°C. Laurdan emission is typically blue (emission around 440 nm) in the gel phase and green (around 490 nm) in the liquid-crystalline phase (33,34). The results are expressed as a generalized polarization function (GPF = $(I_{440} - I_{490})/(I_{440} + I_{490})$), which quantifies the emission spectral changes of the probe, sensitive to the extent of water dipolar relaxation processes in lipid bilayers. It is important to remark that our GPF measurements do not involve the use of polarizers, as in the polarization function described previously the relative parallel and perpendicular orientations of the polarizer are replaced by the intensities at the blue and red edges of the emission spectrum. In some of the spectra shown (i.e., see Fig. 3 *B*), a marginal contribution of the Raman scatter peak of water can be seen as a small maximum at 425 nm, as a consequence of the limited concentration of sample available in the case of LBPs. This was subtracted before calculating the intensities contributing to GPF. Fluorescence of intracellular LBs was measured with an inverted microscope (Zeiss 35, Oberkochen, Germany) equipped with a Polychrome V Monochromator (TILL Photonics, Planegg, Germany) and a microscopic stage

T-controller (Tempcontrol 37, Zeiss). Excitation light was directed through a 420 nm dichroic mirror into a Zeiss Plan-Apochromat 100× NA 1.4 oil objective. Fluorescence images were taken separately by using two band-pass filters centered at 435 ± 5 and 488 ± 6 nm, respectively, and a cooled 12-bit charge-coupled device-camera (PCO-Sensicam, Germany) operated at an acquisition rate of 1 frame/3 s and a binning factor of four. The optical properties of the microscope including the filter sets were cross-calibrated against the spectral output of a multiplate-spectrophotometer (Tecan M200pro, Männedorf, Switzerland) using Laurdan and DMSO as a reference. When transferred to the microscope, the same probe yielded a difference in the GPF values, in particular a much higher 488/435 nm signal intensity ratio. This difference is due to a difference in the instrument's optical properties including the excitation source, all filter sets, and optical components (e.g., objective). Thus, we introduced an empirical correction factor for 488 nm to calibrate the GPF values obtained from the microscope against those measured by the spectrophotometer. Thus, after subtraction of image background, the GP formula was modified to be GPF = $(I_{440} - 0.25 \times I_{490})/(I_{440} + 0.25 \times I_{490})$. Image and data analysis from fluorescence measurements obtained from individual LBs were performed with ImageJ and Microsoft Excel. For the Laurdan image presentation (Fig. 1 *C*), the GPF function was calculated from the intensity corrected images using the mathematical image functions implemented in ImageJ. At least 50 different LBs in at least six independent experiments were measured and averaged to obtain the data presented in the figures.

IR spectroscopy

Oriented multilayers were formed by slow evaporation of 100 μg of NS, OE, or LBPs suspensions under ambient air, yielding a semidry film still bearing residual hydration water molecules at the surface of a germanium plate (35). The recorded spectra were corrected for atmospheric water absorbance interferences by subtracting a reference atmospheric water spectrum. Attenuated total reflection infrared (ATR-FTIR) spectra were recorded in the double-sided, forward-backward mode on a FTIR Bruker IFS 66/R spectrophotometer (Ettlingen, Germany) equipped with a liquid nitrogen cooled mercury cadmium telluride detector at a resolution of 2 cm^{-1} and with an aperture of 3.5 mm. The spectrometer was continuously purged with dry air (15 l/min) to minimize the contribution of atmospheric water. The internal reflection element was a trapezoidal germanium ATR plate (52 × 20 × 2 mm; ACM, Villiers St Frédéric, France) with an aperture angle of 45° yielding 30 internal reflections. The orientation of multilayer membrane arrays was confirmed upon calculation of the dichroic absortion ratios, as described elsewhere (35). The thermotropic behavior of the samples within a range from 15 to 50°C was characterized analyzing the asymmetric stretching of the CH_2 vibration region, which is sensitive to *trans*-gauche isomerization of the lipid chains. To investigate the potential lyotropic polymorphism present in the samples, the region corresponding to CH_2 bending vibration, sensitive to the presence of nonlamellar phases, was also analyzed. Data processing was performed with the software MATLAB R12 Kinetics (The MathWorks, Natick, MA), generously provided by Dr. Erik Goormaghtigh, from Universite Libre de Bruxelles. Baseline corresponding with the crystal absorption in the absence of sample and the atmospheric water contribution were subtracted as described (36). The corrected spectra were smoothed by apodization of its Fourier transform by the Fourier transform of a 4 cm^{-1} Gaussian line shape. The precise position of the different bands was estimated from the second derivative spectra.

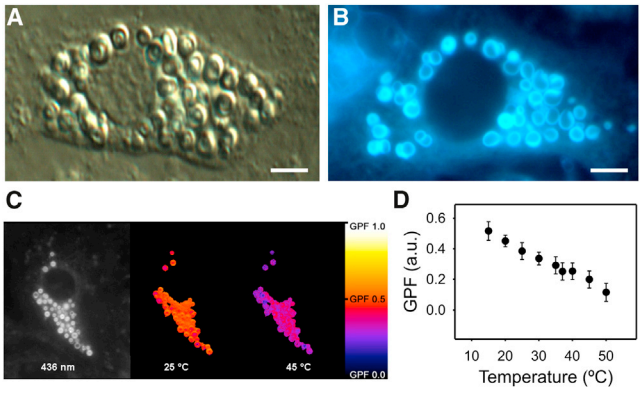

FIGURE 1 Laurdan fluorescence in living rat ATII cells. (*A*) A single ATII cell imaged by differential interference contrast microscopy, displaying its characteristic cytoplasm crowded with lamellar bodies. (*B*) Laurdan fluorescence suggesting progressive labeling of the lamellar body membranes from outer to inner locations. This illustrative image has been acquired with an RGB camera at 360 nm fluorescence excitation and >420 nm emission. (*C*) GPF representation in a single ATII cell evidencing the sensitivity of LB membranes to temperature-dependent structural changes. (*Left*) Black-and-white image captured at 25°C and 463 nm emission. (*Center and right*) GPF image calculations of the same cell when heated from 25 to 45°C. GPF values are presented as color coded (*scale bar*). (*D*) Plot of the thermotropic profile of GPF in intracellular LBs. Scale bars in (*A*) and (*B*) represent 5 μm. Data shown are means ± standard deviation from in total 88 single LBs and 10 independent experiments. To see this figure in color, go online.

Polarization microscopy

Polarization microcopy was performed with an inverted microscope (Zeiss 35) equipped with a Plan-Apochromat 100× NA 1.4 oil objective and crossed polarizers placed between the bright field condenser and the rear aperture of the objective.

Giant unilamellar vesicles preparation

Aliquots of suspended LBPs were incubated with the fluorescent probes Bodipy-PC and DiIC18 (Molecular Probes, Eugene, OR) diluted in an aliquot of DMSO, as described previously, for 1 h at 45°C (probe/phospholipid = 1% mol/mol). For the electroformation of giant unilamellar vesicles (GUVs) composed of labeled-LBPs, 5 μl of an aqueous suspension of LBPs were spread on the surface of indium-tin oxide-coated glass slides as small drops and dried under a stream of N_2, avoiding a complete dehydration of the sample to maintain membrane integrity. Sufficient volume of a buffered solution containing 5 mM Tris and 20 mM NaCl was added to a chamber composed of two conductor glass slides separated by a Teflon spacer of 1 mm and sealed with vinyl paste (CritoSeal; Leica BioSystems, Wetzlar, Germany). The chamber was connected to a function generator (Digimess FG 100, Nürnberg, Germany) and a low frequency AC field was applied using the following sequence: 1) From 0 to 1.5 V, increasing 250 mV every 5 min, with a frequency of 500 Hz; 2) 1.5 V for 1 h, at 500 Hz; and 3) from 500 Hz to 0 Hz, reducing 100 Hz every 10 min. After vesicle formation, the AC field was turned off, and the vesicles were collected with a pipette and transferred to a plastic tube. GUV preparations were observed under a fluorescence upright microscope at 37°C (Leica DM-4000B) equipped with the appropriate fluorescence filters for Bodipy-PC and DiIC18 fluorescence (maximum fluorescence emission at 488 and 543 nm, respectively) and connected to a cooled digital camera (model C10600-10B ORCA-R2, Hamamatsu, Herrsching am Ammersee, Germany).

Atomic force microscopy (AFM) of LBP suspensions

Suspensions of secreted LBPs were directly deposited on top of a freshly exfoliated mica substrate at 37°C and the sample left until solvent evaporation. The AFM images were obtained with a Multimode Nanoscope IIIA

equipped with a type E scanner (Veeco Instruments, Santa Barbara, CA), operated in tapping mode. Tips used were RTESP phosphorus (n) doped silicon probes with a typical radius of >10 nm, nominal spring constant of 40 mN/m, and resonance frequency between 266 and 309 KHz. Topography and phase images were recorded from each sample with 256 scan lines and a frame rate of 0.5 Hz.

Adsorption kinetics assay

Surfactant materials were stained with Bodipy-PC (probe/surfactant = 1% mol/mol) for 1 h at 45°C. Accumulation of surfactant at the interface was evaluated in 96-well microtiter plates as described by Ravasio et al. (37) in a FLUOSTAR Optima microplate reader (BMG Labtech, Offenburg, Germany). Briefly, wells were filled with a solution containing 5 mg/ml of the strongly light-absorbing agent BB, and labeled-surfactant samples (20 μl and 0.5 μg/well) were injected with a multichannel pipette at the bottom of the wells (100 μl final volume). Time 0 for measurements was considered at the moment the whole plate was introduced into the reader, thermostatized, and shaken. After orbital shaking, fluorescence coming from stably surface-adsorbed material was measured by the instrument, whereas fluorescence coming from nonadsorbed complexes was quenched by BB. To evaluate the inhibitory effect of plasma proteins or meconium cholesterol on the adsorption of surfactant materials, experiments were also performed in the presence of increasing concentrations of human serum or meconium, respectively. Values were compared after 60 min of adsorption, because in the standard assay of a good surfactant, adsorption reaches near maximum after around 60 min; kinetics are then normally stabilized, and longer times do not make a real difference. In contrast, inactivated or less active surfactant takes longer to reach maximum adsorption and therefore can be detected as less active by comparing readings at 60 min. If inhibition is only producing a slower adsorption, the measurements at much longer times may not actually reflect such a different behavior. Data in these experiments are presented as the average of three replicates with their standard deviation, in relative fluorescence units (RFU) corrected by subtraction of the measured background (RFU-Bg).

Statistical analysis

Pictures (see Figs. 1, 5, and 6) are representative images after observing several independent experiments. Data (see Figs. 3, 4, and 7) represent means ± standard deviation after averaging three independent experiments. Number of experiments and LBs counted to obtain data (see Figs. 1 and 2) are indicated at the legends. Statistical differences between groups were analyzed using the Student's *t*-test. Significant different values were indicated with *($p < 0.05$) and **($p < 0.01$).

RESULTS

Membrane thermotropic properties

To evaluate packing and hydration properties of the native surfactant forms we took advantage of the spectroscopic features of the probe Laurdan, which is sensitive to the hydration level of the lipid headgroup region and so detects changes in membrane phase properties (38). We started our investigations in isolated, intact rat ATII cells (Fig. 1 *A*), the source of pulmonary surfactant, where we found that staining of intracellular LBs by Laurdan was extremely time- and temperature-dependent (Fig. 1 *B*). Laurdan labeling was observed to progress with time, as the probe diffused progressively into deeper regions of packed LBs, and staining occurred faster at 37°C than at 25°C.

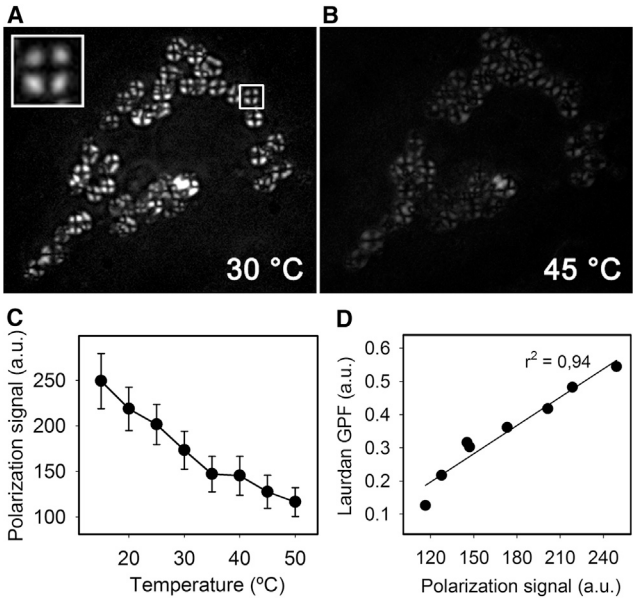

FIGURE 2 Polarized light microscopy of lamellar bodies. (*A*) Single ATII cell imaged by polarized light microscopy. LBs appear as bright, birefringent structures with a central extinction cross (*inset*), whereas other cellular structures remain invisible. (*B*) The increase in temperature leads to a disappearance of the polarization signal. (*C*) Plot is showing the inverse correlation between polarization signal and temperature. (*D*) Plot is demonstrating the correlation between temperature-dependent polarization intensity and the temperature-dependent GPF of Laurdan. Data shown are means ± standard deviation from in total 60 single LBs and six independent experiments.

At 37°C and after 1 h of incubation, most of the probe accumulated close to the external limiting membrane of LBs, whereas diffusion of the probe into deeper layers occurred at prolonged incubation times (3 h) (not shown). As obvious from Fig. 1, LBs are the main or even exclusive site of Laurdan accumulation and individual LBs show a consistent spectral emission of Laurdan with only small differences between lipid ordered (*blue*) and lipid disordered (*green*) states. The thermotropic phase behavior of these LB membranes was tested by applying an incremental, linear increase in T (15 to 50°C) to the stained cells (Fig. 1, *C* and *D*), demonstrating a relatively high dehydrated and packed state below and even above physiological temperatures. At 25°C, LB membranes showed GPF values of around 0.4, similarly to what has been previously reported for condensed pure dipalmitoylphosphatidylcholine (DPPC) layers and significantly higher than those obtained from expanded fully hydrated palmitoyloleoylphosphatidylcholine (POPC) bilayers and monolayers, which display GPF values around −0.2 at the same temperature (32). At 45°C, GPF in intracellular surfactant membranes still remained in positive values of around 0.2 (dehydrated, condensed packing) compared to the fairly expanded and hydrated character of DPPC, POPC, or

DPPC/PG bilayers, which exhibit values below 0 at equivalent temperatures (36).

To gain additional insight into structural features of the lipid assemblies in LBs we examined living ATII cells by incident polarized light microscopy (Fig. 2). The obvious and strong anisotropy of intracellular LBs strongly suggests an ordered, liquid-crystalline assembly of the surfactant molecules. We further hypothesize, due to the regular extinction cross visible within individual LBs, that the reason of optical anisotropy is caused by the radial-symmetric orientation of the phospholipid acyl chains, whereas the intensity of anisotropy may be determined by either the amount of bilayers per unit of volume and/or the degree of molecular alignment of the acyl chains with respect to the orientation of the polarized light wave front (Fig. 2 *A* and *B*). Indeed, the relationship between signal intensity and temperature was shown to be inverse, as the polarization intensity decreased with a rise in temperature (Fig. 2, *B* and *C*). In summary, the thermotropic profiles obtained from polarization microscopy and Laurdan fluorescence were comparable, and even showed a linear correlation (Fig. 2 *D*). In contrast to LBPs, whole NS only exhibit diffuse signals under the polarization microscope, suggesting that most structures have been at least partially unpacked, losing a substantial fraction of their original order.

Laurdan fluorescence was examined to test for differences between released LBPs, native surfactant membranes, and membranes reconstituted from its organic extracts (Fig. 3). NS and OE exhibited a typical broaden phase transition, from an ordered (*blue emission*) to a disordered state (*green emission*), ending slightly above 37°C (see also Laurdan spectra of membranes reconstituted from OE, Fig. S1 in the Supporting Material). However, released LBPs showed a significantly less pronounced GPF change upon the same thermal treatment, maintaining a blue emission throughout the entire T-range up to unphysiologically high temperatures, similar to that obtained with intracellular LBs (Fig. 3 *C*). Thus, intracellular LBs as well as secreted LBPs exhibit an apparently more limited phase transition, which is different from that exhibited by NS or OE membranes. Nevertheless, when compared intracellular and freshly released LBPs at high temperatures such as 50°C, the latter ones exhibited even higher GPF values (0.11 in intracellular LBs—see Fig. 1 *D* versus 0.32 in LBPs), demonstrating a striking condensed and dehydrated character, at least in the headgroup membrane region into which Laurdan has been partitioning.

The ATR-FTIR spectra also evidence differences in the thermotropic behavior and structural organization of lipid phases in LBPs compared to NS or OE membranes (Fig. 4). These two materials exhibit an almost identical thermotropic transition ending at 35–37°C, characterized by a small but consistent shift of the CH_2 asymmetric stretching band to higher wavenumbers. LBPs exhibit a particular thermotropic profile shifted to substantially higher wavenumbers, and their T_m is increased in comparison with that of NS or OE membranes (Fig. 4 *A*). A similar shift to higher wavenumbers of the symmetric strechting band was also observed in spectra of LBPs (see Fig. S2). The increase of wavenumber in the CH_2 stretching bands upon heating above T_m is attributed to the presence of gauche conformers along the acyl chains (39–41). The frequency of the LBPs IR absorption band is shifted to a higher wavenumber than observed in natural surfactant, indicating more intrinsically disordered acyl chains in LBPs (Fig. 4 *B*). On the other hand, CH_2 bending bands are sensitive to hexagonally packed hydrocarbon chains, and therefore to phase organization (40). LBPs display displaced bands with respect to the spectra of membranes of NS or its OE, suggesting the potential presence in LBPs of nonlamellar lipid phases (Fig. 4 *C*). A shift toward a higher wavenumber of the frequency of the C=O strechting band in the spectra of LBPs with respect to the spectra from NS or its OE (1740 vs. 1739 cm^{-1}, see Fig. S2 in the Supporting Material) could be also taken as indicative of the existence of nonlamellar phases (40).

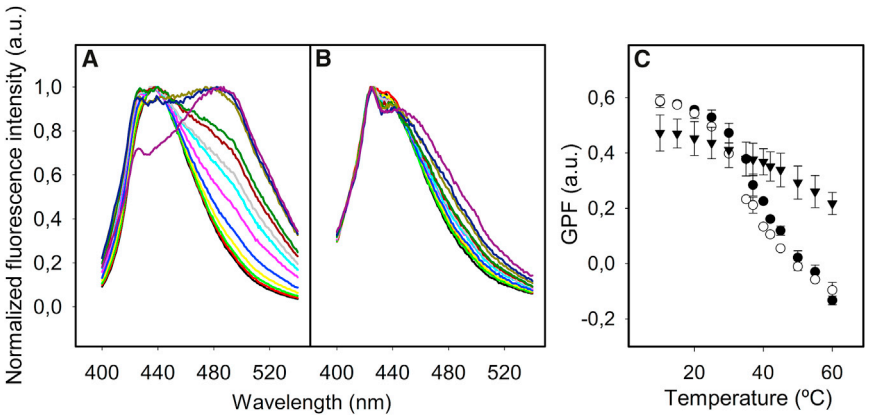

FIGURE 3 Thermotropic profile of secreted lamellar bodies in comparison with surfactant membranes purified from whole lung as measured by Laurdan spectroscopy. Fluorescence emission spectra of Laurdan in suspensions of NS membranes purified from BAL (*A*) or suspensions of secreted LBPs from rat ATII cells (*B*) recorded at 10°C (*black line*), 15°C (*red line*), 20°C (*light green line*), 25°C (*yellow line*), 30°C (*light blue line*), 35°C (*pink line*), 37°C (*turquoise line*), 40°C (*gray line*), 42°C (*maroon line*), 45°C (*dark green line*), 50°C (*light brown line*), 55°C (*dark blue line*), and 60°C (*purple line*). Note that the small peak at 425 nm just comes from the remaining contribution of the Raman scatter peak of water. (*C*) Thermotropic profiles of the GPF of Laurdan fluorescence in NS membranes (*open circles*), membranes reconstituted from organic extract of NS (OE) (*solid circles*), and LBPs (*solid triangles*). Data shown are means ± standard deviation after averaging data from three independent experiments. To see this figure in color, go online.

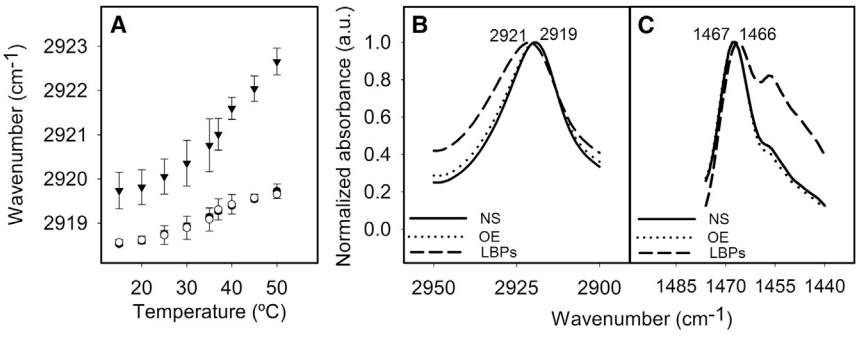

FIGURE 4 ATR-FTIR spectroscopy of surfactant preparations. (*A*) Thermotropic behavior of NS membranes (*open circles*), membranes reconstituted from its OE (*solid circles*), and secreted LBPs (*solid triangles*), as sensed by the wavenumber shift of the CH_2 asymmetric stretching IR bands. (*B* and *C*) ATR-FTIR spectra of NS (—), OE (· · · · ·), and LBPs (- - -) membranes at spectral regions sensitive to the CH_2 asymmetric strechting band (*B*) or to the CH_2 bending band (*C*). Numbers indicate the wavenumber at the maximum of each peak to highlight the shift between the different surfactant materials. Data shown in (*A*) are means ± standard deviation from three independent experiments.

Lateral organization of membranes derived from LBPs

To examine the lateral phase structure of LBPs we transformed them into GUVs and introduced Bodipy-PC and DiIC18 as domain-sensitive fluorescent probes (Fig. 5). Previous work showed that NS membranes could be transformed into GUVs while preserving their lateral structure of segregated ordered/disordered phases (42). The particular round shape of the segregated domains as well as the partition properties of the two fluorescent probes suggest that the lateral organization of vesicles made of LBP material also corresponds to a fluid ordered/fluid disordered phase coexistence (Fig. 5 *A*). When the vesicles adsorbed onto the glass support (Fig. 5 *B*), a flat membrane layer was created, with a core-like region surrounded by an area of more disordered material. This suggested that adsorption of membranes onto the glass surface is initiated from the disordered phases.

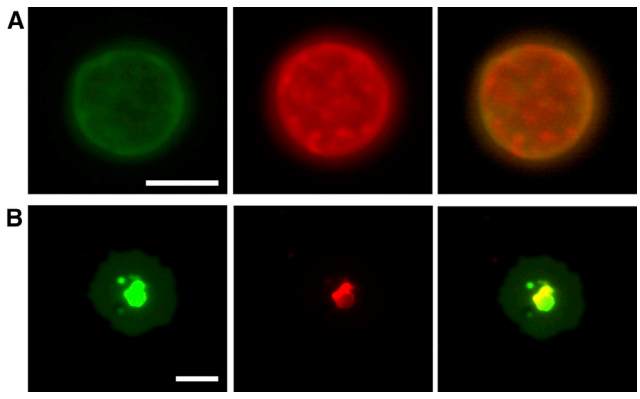

FIGURE 5 Lateral structure in membranes of GUVs prepared from secreted lamellar bodies. GUVs were observed before (*A*) and after their spontaneous adsorption and spreading on glass surfaces (*B*). GUVs were labeled with the lipophilic fluorescence probes Bodipy-PC (*green*, *left panel*) and DiIC 18 (*red*, *central panel*). Merge of both channels is displayed on the right. Rounded red areas in the images correspond to fluid-ordered regions, and the green background to fluid-disordered phases. The scale bars correspond to 5 μm in (*A*) and 10 μm in (*B*), respectively. To see this figure in color, go online.

Nanostructure of adsorbed LBPs

To further explore the lateral structure of the membranes constituting LBPs at submicrometer and nanometric scales we examined their organization by AFM. The study of NS membranes by this technique had confirmed the lateral segregation of ordered/disordered regions seen by fluorescence (42) Fig. 6 shows AFM images obtained from those structures LBPs are forming upon spontaneous adsorption and spreading onto mica supports. In Fig. 6 *A* homogeneous membranous patches with round protruding boundaries are observed. These areas contain a central core displaying a particular pattern composed of structures of different heights. Topological analysis shows that the distribution of heights observed in the central core is more heterogeneous than the height distribution observed in the surrounding area. The central area is magnified in Fig. 6 *B*, revealing numerous well-defined submicron-sized structures with similar diameters (around 0.1 μm) and a height of around 7–8 nm with respect to the general lipid patch and distributed with certain regularity (distanced 0.1 μm with respect to each other). With a minor proportion, other structural organizations were observed as seen in Fig. 6 *C*, which shows a membrane patch with similar morphology but without the presence of a distinguishable central area and displaying various nanosized areas with at least four different levels of height. In general terms, the structure of the membrane layer formed upon adsorption of LBPs onto mica surfaces had a higher level of complexity, with numerous 3D membrane protrusions, than observed in surface SN layers (42). This confirms that, although adsorption processes of surfactant onto solid supports may be very different to those occurring at air-liquid interfaces, the study of the behavior of surfactant structures spread onto glass or mica may be useful to explore intrinsic features that are difficult to observe in situ.

Adsorption properties and resistance to inhibition

To investigate the interfacial adsorption properties of LBPs in the presence of inhibitory agents, we used a method

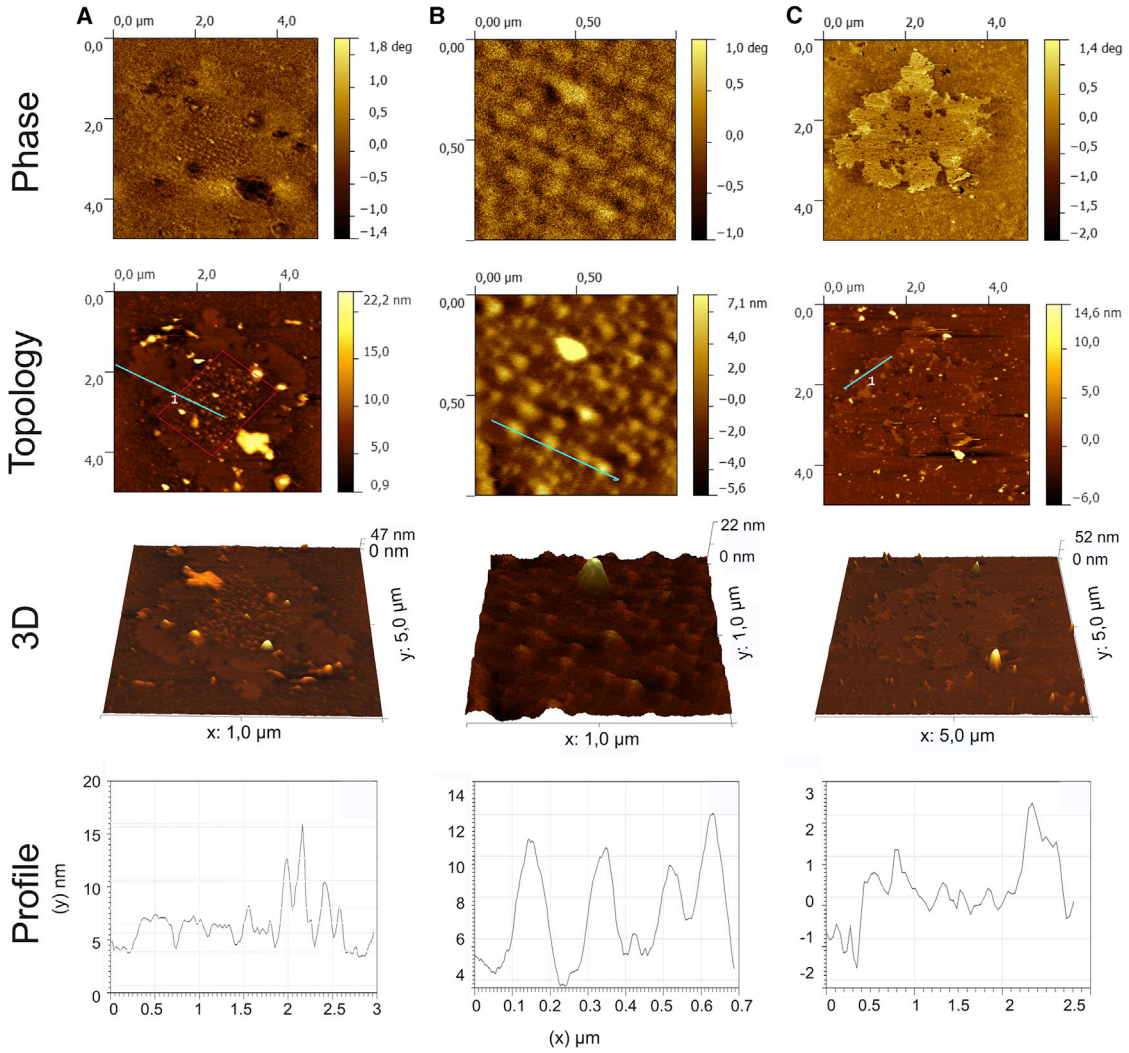

FIGURE 6 Nanostructure of membranes from surface adsorbed LBPs. AFM scanning images have been taken from LBPs adsorbed onto mica surfaces. Phase contrast mode and topology images, tridimensional projections, and topological profiles are compared at different magnifications. (*A*) Images of a 5×5 μm surface region. (*B*) Magnification from the area covered in (*A*) to scan a 1×1 μm surface region. (*C*) AFM image of a 5×5 μm region covering a condensed-like domain such as those seen in the GUV fluorescence experiments.

previously developed in our laboratory that allows evaluation of the amount of surfactant material accumulating at the interface and the resistance of the formed surface films and associated structures against mechanical agitation (37). The deleterious effect of serum proteins and meconium has been previously shown to cause a significant impairment of the surface properties of surfactant, associated with severe respiratory disorders such as acute respiratory distress syndrome or meconium aspiration syndrome, respectively (43,44). In Fig. 7, adsorption kinetics of comparable quantities of suspensions of NS (*left panel*), its reconstituted OE (*middle panel*), or LBPs (*right panel*) have been assessed in the presence of increasing amounts of serum (Fig. 7 *A*) or meconium (Fig. 7 *C*), respectively. The results show that all materials reach the interface quickly and remain stably associated with it, while their exposure to increasing concentrations of either of the two inhibitory agents produces a progressive reduction in the amount of surface-associated material. However, LBPs show a marked resistance to inhibition, displaying significantly better adsorption kinetics than native surfactant membranes in the presence of equivalent concentrations of inhibitory agents (Fig. 7, *B* and *D*).

DISCUSSION

The assembly of lung surfactant membranes in the LBs of alveolar type II cells requires the ATP-driven action of ABCA3 transporters. This leads to hypothesize that the energy expenditure during LB biogenesis confers an energy-loaded state to the surfactant complexes, which might explain the remarkable efficiency by which released LBPs avidly transform into an interfacial film (24). In contrast, NS complexes purified from BALs have been usually considered as the most representative surfactant material,

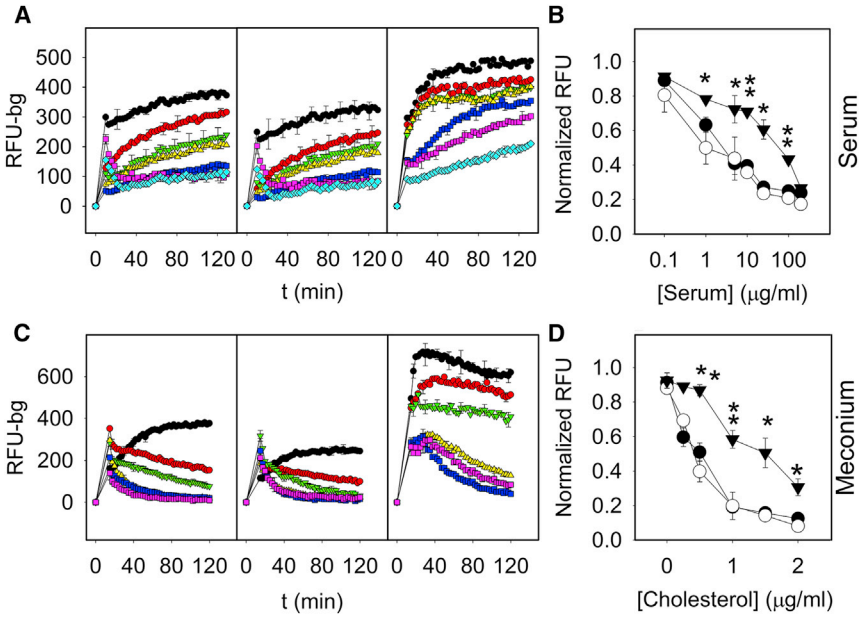

FIGURE 7 Resistance to inhibition of the interfacial adsorption properties of surfactant preparations. Dose-dependent inhibitory effect of human serum proteins (*A* and *B*) or meconium (*C* and *D*) on the adsorption kinetics of NS (*left*), membranes reconstituted from its OE (*center*), and LBPs secreted from rat ATII cells (*right*). Serum protein concentrations were 0 (*black circle*), 1 (*red circle*), 5 (*green inverted triangle*), 10 (*yellow triangle*), 25 (*pink square*), 100 (*blue square*), and 200 (*turquoise diamond*) μg/ml and are presented using a logarithmic scale. Cholesterol concentrations in meconium were 0 (*black circle*), 0.25 (*red circle*), 0.5 (*green inverted triangle*), 1 (*yellow triangle*), 1.5 (*blue square*), and 2 (*pink square*) μg/ml. Right panel summarizes serum protein (*above*) and meconium cholesterol (*below*) dose-response effects on the amount of adsorbed material. Fluorescence values were taken after 60 min of adsorption of NS (*open circles*), OE (*solid circles*) or LBPs (*solid triangles*). Adsorption efficacy in terms of amount of adsorbed material into the surface was significantly higher in the case of LBPs than in NS or its OE at elevated concentrations of inhibitory agents. Data shown are means ± standard deviation after averaging data from three independent experiments. Asterisks indicate statistically significant differences ($p < 0.05$) of LPBs versus NS. To see this figure in color, go online.

a sort of gold standard, for defining structure-function determinants and optimal surfactant functions. However, taking into account that the isolation procedure is collecting material from very different regions of the respiratory tract (e.g., bronchioli) and that this material may contain the product of different states of metabolic and physical conversions (i.e., already exposed to an air-liquid interface or even recycled), the resultant samples may consist only partially of the functional active fraction secreted into the lung alveoli. In fact, previous studies of our group provided evidence that interfacial films formed by freshly secreted LBPs have significantly different structure and properties than films formed by whole natural surfactant purified from animal lungs (24), which could also contain already spent or partly inactivated material.

Our results are consistent with LB membranes possessing a particular highly efficient structure, in terms of producing, once reaching the air-liquid interface, a rapid formation of stable surface films, both in the absence and presence of inhibitors. In the presence of equivalent concentration of serum, LBPs always led to accumulation of larger amounts of material at the interface than NS or the membranes reconstituted from its OE. The membranes constituting freshly secreted LBPs retain an apparently highly dehydrated and packed state in comparison with NS or OE, at least with respect to the membrane regions sensed by Laurdan, despite the fact that LBPs are diluted and fully hydrated as a whole, and that membranes in LBPs are fully permeable to polar molecules like the probe FM1-43. This is astonishing because in NS, a highly dehydrated and packed state can only be seen by applying a lateral compression (32). This observation is also consistent with previous morphological descriptions in which released LBPs appear as dense particulate entities, which retain a highly packed character until contacting the air-liquid interface (22). In addition, it also reflects consistence with the observation of our group that the efficiency in surfactant performance at the interface is related to the propensity of surfactant layers to reach highly dehydrated states (32). Interestingly, the staining of intracellular LBs by Laurdan slightly differed among individual LBs within the same cell (see for instance the *left panel* of Fig. 1 *C*), which could reflect the coexistence of different stages in biogenesis and maturation of these organelles. Some LBs are completely stained by Laurdan, whereas others are just stained in layers closer to the external membrane (see *individual LBs* in Fig. 1 *B*). These differences in Laurdan staining likely reflect differences in the packing and membrane accumulation state affecting the accessibility of the probe. Of importance, though, Laurdan revealed a highly dehydrated state of the surfactant lipids in LBs (Fig. 1 *D*) and a thermotropic profile that was similar to that of LBPs (Fig. 3 *C*). Furthermore, the thermotropic profile as revealed by Laurdan spectroscopy reveals a striking similarity to the changes obtained by polarization microscopy. Although Laurdan fluorescence is most likely providing information about lipid packing density and hydration, and polarization microscopy is most likely providing information about periodical molecular organization, it can be assumed that both inform essentially about the same phenomenon, the transition from ordered to disordered states. Polarization microscopy, however, is noninvasive and thus served as an acceptable positive control for the use of

Laurdan as an invasive lipophilic probe. It is known that anisotropic lipids forming crystal-like structures are able to produce birefringence patterns under polarized light (45). Considering this, we interpret that the optical anisotropy of LBs is probably the result of the radial-symmetric orientation of the phospholipid acyl chains and that LBs exist in a liquid-crystal arrangement at physiological temperatures. As a matter of fact, the preponderance of anisotropy reflected in these cross signals has been observed in other lipid preparations being also associated to smectic liquid-crystalline states (46). In addition, the fact that the polarization signal diminished upon heating toward an optically isotropic state, but increased again after cooling (not shown), could be consistent with a reversible kind of structural reorganization such as a true phase transition. Previous studies revealed that LBs appear to be under mechanical tension, which is partially relieved when the hemifusion state between LB limiting membrane and the pneumocyte plasma membrane is reached (47). Early fusion events also produced a substantial reduction of the cross signals in secreting LBs (not shown), indicating that the exposure of the outer surface of secreted LBPs to the extracellular environment could be a step promoting the acquisition of the competent stage for LBPs to adsorb efficiently at the interface.

ATR-FTIR thermotropic profiles also revealed temperature-dependent changes in lipid packing and lipid order, without the necessity of introducing extrinsic probes. Again, the thermotropic profile of LBPs is significantly different from those of NS membranes or membranes reconstituted from its OE. The position of the CH_2 asymmetric stretching IR absorption band, which is sensitive to conformation, shifted upon heating above T_m, which is attributed to the presence of gauche conformers along the acyl chains (39–41). In LBPs, the frequency of the band is shifted to significantly higher wavenumbers than observed in NS, indicating more intrinsically disordered acyl chains. This higher disordered state of the acyl chains in LBPs as determined by ATR-FTIR is apparently in conflict with the results obtained by the Laurdan measurements, which demonstrated a higher packing and lower hydration. However, these inconsistencies could be conciliated considering the possible presence of nonlamellar phases (40). We examined the IR spectra at the CH_2 bending absorption band, which is dependent on acyl chain packing and conformation and therefore sensitive to the possible presence of nonlamellar phases (39,48). This band also reflects important differences between LBP membranes and both NS and its OE, which are known to be organized constituting two lamellar phases with different thicknesses, as observed by small-angle x-ray scattering (49). Recently, it has been proposed that nonlamellar phases might indeed exist in surfactant lipid complexes and that these phases could be involved in the interconnection of the active surface film with multilayered structures acting as a surfactant reservoir at the aqueous subphase (50). By using lipid model systems, it has also been shown that the surfactant proteins SP-B and SP-C promote formation of cubic phases (50,51). Furthermore, surface-active lipids have been shown to facilitate the formation of hexagonal H_{II} phases (52), highlighting the importance of lipid polymorphism in surfactant function. Unfortunately though, ATR-FTIR does not provide sufficient structural information to definitely prove or disprove the presence of particular lipid phases as could be the case for x-ray diffraction or P^{31} NMR. These techniques could not be applied to study LBP samples due to the extremely limited amount of LBPs that can be collected from isolated cells.

Considering the complex composition of lipids and proteins in lung surfactant, the role of phase coexistence has already been suggested as a key feature in functional terms (42,53). Our results obtained upon examination of the lateral phase structure of intact GUVs prepared from LBP membranes are consistent with previous reports from Ravasio et al. (24) who demonstrated that the films formed by adsorbed LBPs spontaneously segregate into both ordered and disordered phases. It is conceivable that the conditions used to convert LBPs into GUVs may induce changes into the structure of surfactant membranes, particularly with respect to the membrane fusion events required to form the large membrane sheets that ultimately constitute the giant vesicles. Still, these experiments confirm that membranes in LBPs maintain the ability to segregate ordered and disordered lipid regions, a hallmark of pulmonary surfactant layers. Examination by AFM revealed that once adsorbed onto supports, LBPs generate structures with two different areas including a central core exhibiting well-defined domains distanced with certain regularity surrounded by flat membrane patches. The prominent domains could be interpreted as the result of the formation of large protruded 3D structures typically observed from LBPs adsorbed on air-liquid interfaces (24), very different than the flat layers formed by SN, both at mica surfaces (42) and at the interface in situ (24). The periodical distribution of the domains present in the core resemble a lattice-like structure and suggests the presence of membrane-associated scaffolds of proteins, imposing these distances. Moreover, the complexity observed in the nanostructure of adsorbed LBPs displays marked differences with respect to the organization of NS membranes visualized under AFM (28).

The unique structural organization of LB membranes seem to be particularly well suited to sustain an efficient formation of surface active films, even in the presence of inhibitory agents such as serum or meconium. The higher adsorptive capacity of LBPs in comparison with whole NS membranes has already been demonstrated (37). Consistent with previous biophysical studies (23,44), we also observed that these inhibitors lead to a dramatic reduction in the accumulation of surfactant material into the air-liquid interface and so reduce its adsorptive capability. Here, we have shown

that freshly secreted LBPs display a significantly higher resistance to both serum proteins and cholesterol than whole NS and complexes reconstituted from its OE. These findings suggest that LBPs are endowed with adsorptive mechanisms that are clearly different from those of NS or its OE. Although the nature and molecular identity of these mechanisms is still enigmatic, this study is putting forward the idea that either a peculiar phase organization in the membranes of LBPs, or the presence of a protein scaffold on the outermost LBP membrane may be part of a mechanism by which an efficient adsorption can occur, even in the presence of strong inhibitory conditions.

The transfer of phospholipid species across the limiting membrane of LBs during their biogenesis is catalyzed by ABCA3 transporters with expenditure of ATP (16). Thus, lipid assembly in LBs is a highly energy-dependent process. We propose that the energy accumulated during biogenesis could convert LBs into a sort of pressurized particles, with phospholipids adopting particular high-energy structures that may include nonlamellar assemblies. This activated structure likely includes a high level of dehydration, which might be promoted both by the high packing created upon accumulation of phospholipids into a limited volume, and as a consequence of osmotic stress induced by the segregation of large protein complexes out from the tightly packed multilamellar arrays. A similar polymer-promoted osmotic stress could be behind the well documented effect of large polymers to induce activation of different pulmonary surfactant preparations, which then become particularly resistant to serum inhibition (44,54). The stability conferred by this internal pressure or mechanical tension could be maintained as long as the external membrane of the secreted LBs is intact. Once reaching the air-liquid interface, the disruption of the external membrane could somehow liberate all the energy accumulated, resulting in the observation of a highly efficient interfacial adsorption, even in the presence of inhibitors. However, once adsorbed and spread, surfactant material would have lost important features of its original activated structure, and could be therefore considered as already spent surfactant. Exposure to the highly oxidative pulmonary airspaces could also led to partial oxidation and further deactivation of the functionally important lipid and protein species in surfactant. All these processes would be responsible for a significant reduction of activity of the average surfactant complexes obtained from lavage compared with those freshly secreted by pneumocytes. The presence of inactivated or spent structures contained in native surfactant has been previously and extensively reported by a number of authors (55–59), although the nature of this activity dissipation has never been fully understood.

The elucidation of the mechanisms involving the assembly of highly active surfactant complexes would be of high relevance for the design of novel therapeutic materials with less susceptibility to inhibition and a higher therapeutic efficiency for the treatment of respiratory pathologies such as the acute respiratory distress syndrome or interstitial lung diseases.

In summary, our results show that pulmonary surfactant membranes as they are assembled and freshly released by the ATII cells display very distinctive features. They are in a highly packed and dehydrated state with an optimized adsorptive performance toward air-liquid interfaces, and with a high intrinsic resistance to inactivation. These features are very different from those of natural surfactant typically isolated from animal lungs and typically used in surfactant research, and could arise from the fact that LBPs are a primordial form in which surfactant is released, still containing the whole complement of lipids and proteins in a possibly unaltered structural configuration. Future investigations will be necessary to unveil this configuration at a molecular level and to apply this knowledge to the design and production of new optimized therapeutic surfactants.

SUPPORTING MATERIAL

Two figures are available at http://www.biophysj.org/biophysj/supplemental/S0006-3495(15)01061-9.

AUTHOR CONTRIBUTIONS

A. Cerrada designed and performed the research, analyzed the data, and wrote the article. T.H. contributed tools, performed the research, and analyzed the data. A. Cruz designed the research, contributed tools, and discussed the data. J. P.-G. designed the research, supervised the project, and wrote the article.

ACKNOWLEDGMENTS

The authors are indebted to Dr. Elena López Rodríguez, for her technical assistance with some of the ATR-IR experiments. They also acknowledge Dr. Nina Hobi for help in obtaining the LBP preparations.

This work has been supported by grants from Spanish Ministry of Economy (BIO2012-30733), the Regional Government of Madrid (S2013/MIT-2807), and the Austrian Science Fund (FWF; P20472).

REFERENCES

1. Perez-Gil, J., and T. E. Weaver. 2010. Pulmonary surfactant pathophysiology: current models and open questions. *Physiology (Bethesda).* 25:132–141.
2. Daniels, C. B., and S. Orgeig. 2003. Pulmonary surfactant: the key to the evolution of air breathing. *News Physiol. Sci.* 18:151–157.
3. Lopez-Rodriguez, E., and J. Pérez-Gil. 2014. Structure-function relationships in pulmonary surfactant membranes: from biophysics to therapy. *Biochim. Biophys. Acta.* 1838:1568–1585.
4. Pérez-Gil, J. 2008. Structure of pulmonary surfactant membranes and films: the role of proteins and lipid-protein interactions. *Biochim. Biophys. Acta.* 1778:1676–1695.
5. Crouch, E., and J. R. Wright. 2001. Surfactant proteins a and d and pulmonary host defense. *Annu. Rev. Physiol.* 63:521–554.
6. Eggleton, P., and K. B. Reid. 1999. Lung surfactant proteins involved in innate immunity. *Curr. Opin. Immunol.* 11:28–33.

7. Sano, H., and Y. Kuroki. 2005. The lung collectins, SP-A and SP-D, modulate pulmonary innate immunity. *Mol. Immunol.* 42:279–287.
8. Olmeda, B., L. Villén, …, J. Perez-Gil. 2010. Pulmonary surfactant layers accelerate O(2) diffusion through the air-water interface. *Biochim. Biophys. Acta.* 1798:1281–1284.
9. Blanco, O., and J. Pérez-Gil. 2007. Biochemical and pharmacological differences between preparations of exogenous natural surfactant used to treat Respiratory Distress Syndrome: role of the different components in an efficient pulmonary surfactant. *Eur. J. Pharmacol.* 568:1–15.
10. Goerke, J. 1998. Pulmonary surfactant: functions and molecular composition. *Biochim. Biophys. Acta.* 1408:79–89.
11. Vanhecke, D., G. Herrmann, …, M. Ochs. 2010. Lamellar body ultrastructure revisited: high-pressure freezing and cryo-electron microscopy of vitreous sections. *Histochem. Cell Biol.* 134:319–326.
12. Wright, J. R., and J. A. Clements. 1987. Metabolism and turnover of lung surfactant. *Am. Rev. Respir. Dis.* 136:426–444.
13. Chander, A., R. G. Johnson, …, A. B. Fisher. 1986. Lung lamellar bodies maintain an acidic internal pH. *J. Biol. Chem.* 261:6126–6131.
14. Ridsdale, R., C. L. Na, …, T. Weaver. 2011. Comparative proteomic analysis of lung lamellar bodies and lysosome-related organelles. *PLoS One.* 6:e16482.
15. Wang, P., N. R. Chintagari, …, L. Liu. 2008. Proteomic analysis of lamellar bodies isolated from rat lungs. *BMC Cell Biol.* 9:34.
16. Ban, N., Y. Matsumura, …, N. Inagaki. 2007. ABCA3 as a lipid transporter in pulmonary surfactant biogenesis. *J. Biol. Chem.* 282:9628–9634.
17. Fitzgerald, M. L., R. Xavier, …, M. W. Freeman. 2007. ABCA3 inactivation in mice causes respiratory failure, loss of pulmonary surfactant, and depletion of lung phosphatidylglycerol. *J. Lipid Res.* 48:621–632.
18. Chander, A., and A. B. Fisher. 1990. Regulation of lung surfactant secretion. *Am. J. Physiol.* 258:L241–L253.
19. Dietl, P., and T. Haller. 2005. Exocytosis of lung surfactant: from the secretory vesicle to the air-liquid interface. *Annu. Rev. Physiol.* 67:595–621.
20. Dietl, P., T. Haller, …, M. Frick. 2001. Mechanisms of surfactant exocytosis in alveolar type II cells in vitro and in vivo. *News Physiol. Sci.* 16:239–243.
21. Mason, R. J., and D. R. Voelker. 1998. Regulatory mechanisms of surfactant secretion. *Biochim. Biophys. Acta.* 1408:226–240.
22. Haller, T., P. Dietl, …, G. Putz. 2004. Tracing surfactant transformation from cellular release to insertion into an air-liquid interface. *Am. J. Physiol. Lung Cell. Mol. Physiol.* 286:L1009–L1015.
23. Hobi, N., G. Siber, …, T. Haller. 2014. Physiological variables affecting surface film formation by native lamellar body-like pulmonary surfactant particles. *Biochim. Biophys. Acta.* 1838:1842–1850.
24. Ravasio, A., B. Olmeda, …, J. Pérez-Gil. 2010. Lamellar bodies form solid three-dimensional films at the respiratory air-liquid interface. *J. Biol. Chem.* 285:28174–28182.
25. Dobbs, L. G., R. Gonzalez, and M. C. Williams. 1986. An improved method for isolating type II cells in high yield and purity. *Am. Rev. Respir. Dis.* 134:141–145.
26. Haller, T., J. Ortmayr, …, P. Dietl. 1998. Dynamics of surfactant release in alveolar type II cells. *Proc. Natl. Acad. Sci. USA.* 95:1579–1584.
27. Taeusch, H. W., J. Bernardino de la Serna, …, J. A. Zasadzinski. 2005. Inactivation of pulmonary surfactant due to serum-inhibited adsorption and reversal by hydrophilic polymers: experimental. *Biophys. J.* 89:1769–1779.
28. Blanco, O., A. Cruz, …, J. Pérez-Gil. 2012. Interfacial behavior and structural properties of a clinical lung surfactant from porcine source. *Biochim. Biophys. Acta.* 1818:2756–2766.
29. Bligh, E. G., and W. J. Dyer. 1959. A rapid method of total lipid extraction and purification. *Can. J. Biochem. Physiol.* 37:911–917.
30. Rouser, G., A. N. Siakotos, and S. Fleischer. 1966. Quantitative analysis of phospholipids by thin-layer chromatography and phosphorus analysis of spots. *Lipids.* 1:85–86.
31. Garcia-Verdugo, I., A. Ravasio, …, T. Haller. 2008. Long-term exposure to LPS enhances the rate of stimulated exocytosis and surfactant secretion in alveolar type II cells and upregulates P2Y2 receptor expression. *Am. J. Physiol. Lung Cell. Mol. Physiol.* 295:L708–L717.
32. Picardi, M. V., A. Cruz, …, J. Pérez-Gil. 2011. Phospholipid packing and hydration in pulmonary surfactant membranes and films as sensed by LAURDAN. *Biochim. Biophys. Acta.* 1808:696–705.
33. Parasassi, T., G. De Stasio, …, E. Gratton. 1990. Phase fluctuation in phospholipid membranes revealed by Laurdan fluorescence. *Biophys. J.* 57:1179–1186.
34. Parasassi, T., G. De Stasio, …, E. Gratton. 1991. Quantitation of lipid phases in phospholipid vesicles by the generalized polarization of Laurdan fluorescence. *Biophys. J.* 60:179–189.
35. Roldan, N., E. Goormaghtigh, …, B. Garcia-Alvarez. 2015. Palmitoylation as a key factor to modulate SP-C-lipid interactions in lung surfactant membrane multilayers. *Biochim. Biophys. Acta.* 1848 (1 Pt A):184–191.
36. Alegre-Cebollada, J., A. Martínez del Pozo, …, E. Goormaghtigh. 2007. Infrared spectroscopy study on the conformational changes leading to pore formation of the toxin sticholysin II. *Biophys. J.* 93:3191–3201.
37. Ravasio, A., A. Cruz, …, T. Haller. 2008. High-throughput evaluation of pulmonary surfactant adsorption and surface film formation. *J. Lipid Res.* 49:2479–2488.
38. De Vequi-Suplicy, C. C., C. R. Benatti, and M. T. Lamy. 2006. Laurdan in fluid bilayers: position and structural sensitivity. *J. Fluoresc.* 16:431–439.
39. Casal, H. L., and H. H. Mantsch. 1984. Polymorphic phase behaviour of phospholipid membranes studied by infrared spectroscopy. *Biochim. Biophys. Acta.* 779:381–401.
40. Lewis, R. N., and R. N. McElhaney. 2013. Membrane lipid phase transitions and phase organization studied by Fourier transform infrared spectroscopy. *Biochim. Biophys. Acta.* 1828:2347–2358.
41. Lotta, T. I., J. A. Virtanen, and P. K. Kinnunen. 1988. Fourier transform infrared study on the thermotropic behaviour of fully hydrated 1-palmitoyl-2-[10-(pyren-1-y) decanoyl]-*sn*-glycero-3-phosphatidylcholine. *Chem. Phys. Lipids.* 46:13–23.
42. Bernardino de la Serna, J., J. Perez-Gil, …, L. A. Bagatolli. 2004. Cholesterol rules: direct observation of the coexistence of two fluid phases in native pulmonary surfactant membranes at physiological temperatures. *J. Biol. Chem.* 279:40715–40722.
43. Lopez-Rodriguez, E., M. Echaide, …, J. Perez-Gil. 2011. Meconium impairs pulmonary surfactant by a combined action of cholesterol and bile acids. *Biophys. J.* 100:646–655.
44. López-Rodríguez, E., O. L. Ospina, …, J. Pérez-Gil. 2012. Exposure to polymers reverses inhibition of pulmonary surfactant by serum, meconium, or cholesterol in the captive bubble surfactometer. *Biophys. J.* 103:1451–1459.
45. Butovich, I. A., H. Lu, …, E. Linsenbardt. 2014. Biophysical and morphological evaluation of human normal and dry eye meibum using hot stage polarized light microscopy. *Invest. Ophthalmol. Vis. Sci.* 55:87–101.
46. Katz, S. S., G. G. Shipley, and D. M. Small. 1976. Physical chemistry of the lipids of human atherosclerotic lesions. Demonstration of a lesion intermediate between fatty streaks and advanced plaques. *J. Clin. Invest.* 58:200–211.
47. Miklavc, P., S. Albrecht, …, P. Dietl. 2009. Existence of exocytotic hemifusion intermediates with a lifetime of up to seconds in type II pneumocytes. *Biochem. J.* 424:7–14.
48. Wallach, D. F., S. P. Verma, and J. Fookson. 1979. Application of laser Raman and infrared spectroscopy to the analysis of membrane structure. *Biochim. Biophys. Acta.* 559:153–208.

49. Bernardino de la Serna, J., R. Vargas, …, J. Pérez-Gil. 2013. Segregated ordered lipid phases and protein-promoted membrane cohesivity are required for pulmonary surfactant films to stabilize and protect the respiratory surface. *Faraday Discuss.* 161:535–548, discussion 563–589.

50. Chavarha, M., H. Khoojinian, …, S. B. Hall. 2010. Hydrophobic surfactant proteins induce a phosphatidylethanolamine to form cubic phases. *Biophys. J.* 98:1549–1557.

51. Chavarha, M., R. W. Loney, …, S. B. Hall. 2012. Differential effects of the hydrophobic surfactant proteins on the formation of inverse bicontinuous cubic phases. *Langmuir.* 28:16596–16604.

52. Perkins, W. R., R. B. Dause, …, A. S. Janoff. 1996. Role of lipid polymorphism in pulmonary surfactant. *Science.* 273:330–332.

53. Casals, C., and O. Cañadas. 2012. Role of lipid ordered/disordered phase coexistence in pulmonary surfactant function. *Biochim. Biophys. Acta.* 1818:2550–2562.

54. Braun, A., P. C. Stenger, …, H. W. Taeusch. 2007. A freeze-fracture transmission electron microscopy and small angle x-ray diffraction study of the effects of albumin, serum, and polymers on clinical lung surfactant microstructure. *Biophys. J.* 93:123–139.

55. Gross, N. J., M. Kellam, …, R. Dhand. 2000. Separation of alveolar surfactant into subtypes. A comparison of methods. *Am. J. Respir. Crit. Care Med.* 162:617–622.

56. Gross, N. J., and K. R. Narine. 1989. Surfactant subtypes of mice: metabolic relationships and conversion in vitro. *J. Appl. Physiol.* 67:414–421.

57. Guthmann, F., R. Haupt, …, B. Rüstow. 1995. Alveolar surfactant subfractions differ in their lipid composition. *Int. J. Biochem. Cell Biol.* 27:1021–1026.

58. Magoon, M. W., J. R. Wright, …, J. A. Clements. 1983. Subfractionation of lung surfactant. Implications for metabolism and surface activity. *Biochim. Biophys. Acta.* 750:18–31.

59. Putman, E., L. A. Creuwels, …, H. P. Haagsman. 1996. Surface properties, morphology and protein composition of pulmonary surfactant subtypes. *Biochem. J.* 320:599–605.